Effect of preparation methods on magnetic properties of stoichiometric zinc ferrite

M A Cobos[a], P de la Presa[a,b], I. Llorente[c], A García-Escorial[c], A. Hernando[a,b], J A Jiménez[c].

a. Instituto de Magnetismo aplicado (UCM-ADIF-CSIC), A6 22,500 Km, 28260 Las Rozas, Spain

b. Dpto Física de Materiales, UCM, Ciudad Universitaria, 28040 Madrid, Spain

c. Centro Nacional de Investigaciones Metalúrgicas (CENIM-CSIC), Avda. Gregorio del Amo, 8, 28040 Madrid, Spain

Corresponding Author: P de la Presa (pmpresa@ucm.es)

Abstract

Synthesis and processing methods can have a significant influence on the physical properties of spinel zinc ferrite since it can produce microstructures characterized by different microstructural parameter such as the arrangement of the ions, lattice parameter, crystallite size and lattice strains (or microstrain). In this work, it has been evaluated the magnetic properties of samples prepared by ceramic synthesis, sol-gel and a third one provided by a ceramic powder supplier. Later, the synthesized samples have been ball-milled for 50 h and compared with a sample prepared by mechanochemical synthesis during 150 h. X-ray powder diffraction (XRD) analysis, performed in order to understand the relation between microstructure and magnetic properties, showed that these four materials are characterized by different values of the microstructural parameters (lattice constant, inversion degree and crystallite size). It was concluded that cation inversion is the most important parameters that can be effective in the deviation of the magnetic properties of zinc ferrite from the properties of the bulk form. Finally, the magnetization curves for the samples milled for 50 h were very similar to the sample prepared by mechanochemical, as expected from the similar microstructural parameters obtained from their XRD patterns. The inversion

degree for these samples varied from 0.56 and 0.61 with saturation magnetization at 5 K around 79.0 emu/g.

Keywords: zinc ferrite, mechanochemical processing, solid state reactions, sol-gel, magnetisation, microstructure

1. Introduction

Structural and magnetic properties of zinc ferrites have been studied by many researchers over the last decades. It has been stablished, that this compound belongs to the $Fd\bar{3}m$ space group and presents a normal spinel structure with Zn^{2+} occupying only tetrahedral A sites, due to their affinity for strong sp^3 bonding with oxygen, and Fe^{3+} ions located at the octahedral B sites.[1, 2] This compound is paramagnetic, with a transition to an antiferromagnetic order around 10 K,[3] in which Zn^{2+} ions with a d^{10} electronic configuration has not magnetic moment while Fe^{3+} B-ions with a d^7 configuration are in a high spin state with an antiferromagnetic order. However, this magnetic structure can be largely modified by the cation exchange between Fe^{3+} ions in the octahedral sites and Zn^{2+} ions in the tetrahedral sites, through the onset super-exchange magnetic interaction between Fe^{3+} - Fe^{3+} ions at A-B sites via the bridging of an intermediate O^{2-} ion.[4] It has been experimentally established that these interaction energies are negative, and hence induce an anti-parallel orientation of the magnetic moments of the Fe^{3+} cations on A and B sites.[5] This cation disorder is also accompanied by the decrease of both unit cell dimension (a) and oxygen parameter (u) that produce a change in the A-O-B cations bond angle.[6] All these microstructural modifications make possible that zinc ferrite can present superparamagnetic or ferrimagnetic behavior at room temperature.[7, 8]

The site occupancy of Zn and Fe ions is temperature dependent,[9] and the equilibrium configuration described before can be re-adjusted at high temperature. This new configuration can be frozen by quenching to room temperature. For this reason, the site occupancy of these ions can depend on the thermal history of the spinel.[10] On the other hand, it has been reported that the particular inversion degree is also dependent on particle size.[11, 12] Since the synthesis process selected determines the thermal history of the material and its particle size, the experimental route used in the preparation of ferrites plays an important role in their properties, and anomalies in the magnetic behavior in samples prepared by various techniques has been reported. Comparing magnetic properties of this material prepared through different synthesis methods (eg. co-precipitation,[13, 14] combustion,[15-17] sol-gel,[18-20] hydrothermal

route,[21-23] solvothermal methods,[24, 25] spray drying,[26, 27] mechanochemical synthesis[28-31]) with the microstructure present, it can be concluded that beside the inversion degree, microstructural parameters like the lattice constant, crystallite size and lattice strains (or microstrain) must be taken in account to understand its magnetic properties.[32-34]

The conventional ceramic methods for the preparation of ferrites consists of a high temperature thermal treatment of an equal molar mixture of ZnO and α-Fe_2O_3 powders. This method is widely used for large scale production of zinc ferrite since allows the production of highly crystalline material at low cost. However, the required long heating schedule at high temperatures can lead to zinc loss and the sintering of the powders forms large and hard agglomerates with particles and grain sizes bigger than the optimal for most of the applications.[35] These compacts have to be ball-milled to achieve a better homogeneity and to reduce the particle size, but by this process it is obtained a broad distribution of size and shape of particles with different morphologies.[36, 37] Besides, contamination of the ferrite powder with the grinding material can result in deviation from the desired stoichiometry.[38]

Sol-gel chemical methods for the preparation of a variety of mixed-metal oxide could present advantages to overcome the most drawbacks of the conventional route in terms of simplicity.[39, 40] The process consists on the preparation of a colloidal suspension of the desired oxide from salts, that is converted into a gel by dehydration. Finally, this gel is calcined without a specific heating or cooling rate to produce the desired ceramic particles.[41] It has been demonstrated that this technique allows to produce oxides with an excellent chemical homogeneity at low processing temperatures.[42] Besides, this technique represents the possibility of producing nano-sized ferrite particles with uniform and narrow size, which can present large differences in properties from bulk materials and, therefore, they can find new areas of applications.

Other fabrication method reported to prepare spinel zinc ferrite nanocrystals with new and unusual properties is the high energy ball milling at room temperature of ZnO and α-Fe_2O_3 powder mixture (mechanochemical synthesis).[43] This technique has the advantage that it can easily be operated and produces large

amounts of nanostructured powders for a short period of time.[44] Besides, this processing allows tailoring magnetic properties of zinc ferrite by producing the desired inversion degree and reducing strains and structural defects introduced by milling through thermal treatments. However, a problem found in nanostructured high-energy milled spinel ferrites is related to its thermal stability owing to their small particle size, non-equilibrium cation distribution,[31] disordered spin configuration,[45, 46] and high-chemical activity.[47] Because of their unstable character, decomposition of zinc ferrite into ZnO and/or hematite may occur as a result of a further thermal treatment.

This work is aimed to understand the relation between microstructure and magnetic properties of ferrites by comparing XRD and magnetic properties measurements performed on samples prepared by the three most common synthesis methods (conventional ceramic, mechanochemical, and sol-gel synthesis) and powders of zinc ferrite supplied by Alpha Aesar. For this goal, changes on microstructural parameters like the lattice constant, inversion degree, crystallite size and lattice strains (or microstrain) were correlated with the temperature dependence of the magnetization under zero-field cooled and field cooled procedure and hysteresis cycles at room and low temperatures measured by SQUID magnetometry. Finally, the effect of ball milling on the structural and magnetic properties of these four samples was investigated since this method can result in an enhancement in magnetization by the elimination of the residual amount of amount of ZnO and/or α-Fe_2O_3 that can be present in the microstructure and also changing the cation distribution and particle size.

2. **Experimental procedure**

Stoichiometric $ZnFe_2O_4$ particle have been processed by four different routes:

a) Conventional ceramic synthesis: a 1:1 molar ratio mixture of ZnO and α-Fe_2O_3 (both 99% purity) supplied by Panreac and Alpha Aesar, respectively, were ground to a very fine powder and then pressed into pellets using a uniaxial press and sintered at 1200 ºC for 24 h. After this treatment, the samples were air cooled to room temperature. The sample is denominated as CS.

b) Sol-gel: $Zn(NO_3)_2$-$6H_2O$ and $Fe(NO_3)_3$-$9H_2O$ were dissolved separately in a stoichiometric ratio of 1:2 in ethanol and ethylenglycol, respectively. Both solutions were mixed with continuous stirring with a magnetic agitator to form a sol by heating at 60 ºC for 8 h. This sol was heated at 120 ºC until it transformed into a dark brown gel. Finally, the dried gel was calcined at 600 ºC for 24 h to obtain a nanosized zinc ferrite powder, following the result of the characterization study performed with the gel. The sample is called SG.

c) As zinc ferrite obtained by the ceramic and sol-gel methods can present some residual amount of amount of ZnO and/or α-Fe_2O_3, a portion of the powder obtained by these methods was mechanically milled to get complete homogeneity. For this goal, the powder was placed in stainless steel vial with 10:1 ball to powder weight ratio keeping milling intensity at 275 rpm for 50 and 38 h, respectively.

d) Mechanochemical synthesis: 10 g of a powder mixture in a 1:1 molar ratio of ZnO and α-Fe_2O_3 (both 99% purity) supplied by Panreac and Alpha Aesar, respectively, was introduced together with stainless steel balls of 10 mm into a stainless steel jar of 250 cm^3 in ball-to-powder weight ratio of 10:1. The milling process was carried out up at room temperature in a planetary ball mill Retsch PM4 working at an average rotation speed of 275 rpm. The milling process was interrupted after 150 h since in a previous work it was confirmed that it is the required time to obtain a single phase.[31] The sample is named MS.

e) This study was complemented with the microstructural and magnetic characterization of 99% purity zinc ferrite supplied by Alpha Aesar. Besides, a certain amount of the powder was mechanical milling under the same conditions as given in c). The sample is denominated as ZFS.

The preparation processes are shown in the following schematic diagram:

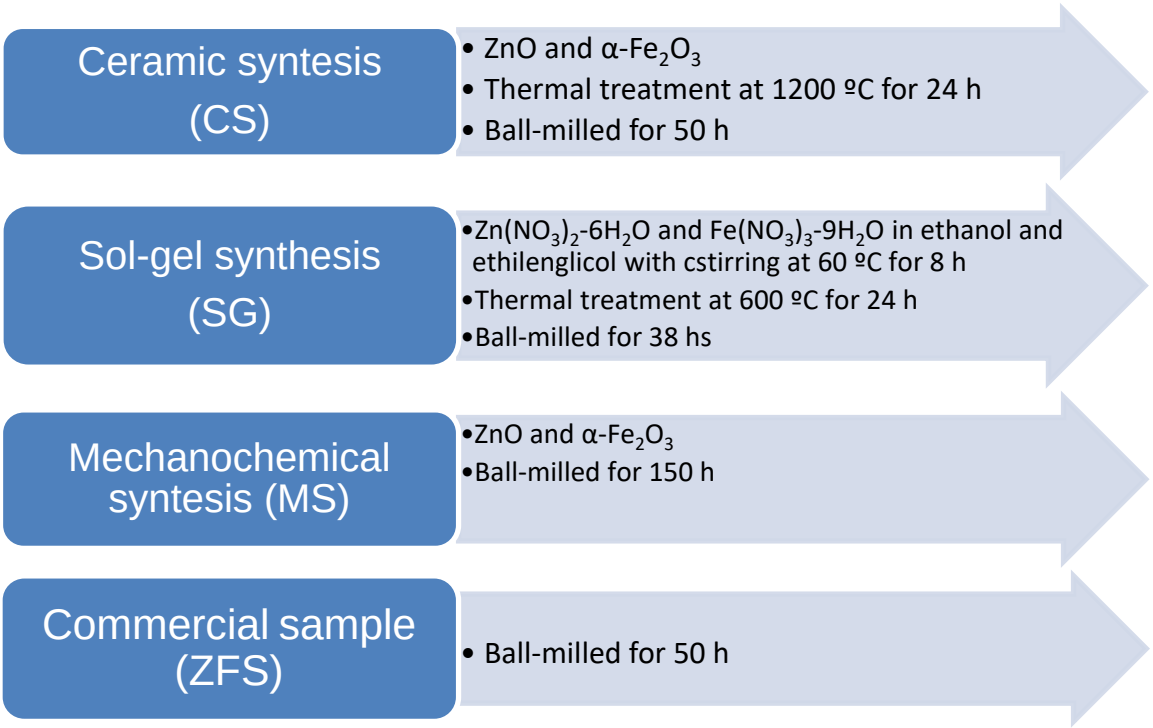

Thermogravimetric analysis (TGA) and differential scanning calorimetry (DSC) measurements of about 10 mg of SG were carried from 50 to 1200 ºC using SDT Q600 V8.3 Build 101 thermal analyzer in Pt crucibles at a heating rate of 10 K/min. From the steps weigh loss temperature observed on the TGA curve during heating, powder of the dried gel was calcined at temperatures ranging from 350 to 600 ºC to understand the removing process of unwanted organic ions. Powder of these calcined samples was mixed with KBr powder to prepare a pellet for Fourier Transform Infrared (FTIR) studies to determine stretching and vibrations molecular modes of organic sources. FTIR absorption spectra, were recorded in the wave-number range between 500 and 4000 cm^{-1}.

Microstructural characterization for the different processing routes was conducted by X-ray diffraction (XRD). XRD measurements were carried out in a Bruker AXS D8 diffractometer equipped with a Goebel mirror and a LynxEye detector. XRD spectra were collected in Bragg-Brentano geometry using Co radiation over a range from 10 to 120º with a step width of 0.01º. The version 6.0 of Rietveld analysis program TOPAS (Bruker AXS) was used to model the

diffraction pattern with the crystallographic information of ZnO, α-Fe_2O_3 and $ZnFe_2O_4$ obtained from Pearson's Crystal Structure databases.[48] The refinement protocol included determination of the following structure parameters for the zinc ferrite: the unit-cell parameters (a), oxygen fractional coordinates (x=y=z), and the degree of inversion δ (constraining the octahedral and tetrahedral sites to keep the sum of the same cations in the two sites to its stoichiometric value). Uncertainties in these three parameters were determined from the standard deviation obtained from the least-squares refinements. Isotropic temperature factors (Biso) used in Rietveld refinements were fixed to the values reported by O'Neill.[9] The determination of crystallite size and lattice strain simultaneously from line broadening of the XRD patterns has been carried out by the double Voigt approach.[49, 50] For this analysis, the instrumental contribution to peak broadening was removed using the diffraction patter of a corundum sample. However, the results obtained for domain size and strain parameters present a limited reliability (ranging from 10 to 20%) associated with a large standard deviation.

Scanning and transmission electron microscopes have been used to determine the particle size. The images used for this task were obtained using a JEOL - JSM 6330F and a JEOL JEM2100, respectively. In order to avoid measurements error during image analysis, the recognition and delimitation of primary particles in agglomerates was performed manually.

Magnetic characterization of the samples as a function of applied field and temperature has been carried out using a standard superconducting quantum interference device (SQUID) MPMS (Quantum Design) magnetometer with the maximum applied field of 5 T. In addition, Physical Property Measurement System (PPMS) Quantum Design Vibrant sample magnetometer (VSM) was also used. Hysteresis cycles have been made at 5 and 300 K at 5 T. Zero field cooled (ZFC) and field cooled (FC) measurements were made at magnetic field of 100 Oe between 5 and 300 K.

3 Results

3.1 Microstructural characterization

The XRD patterns of the precursor prepared by sol-gel showed the presence of many sharp diffraction peaks, but none of them could be associated to the zinc ferrite (see Fig. 1a). The XRD patterns of sampled calcined at 300, 425 and 550 ºC for 2 h (Fig. 1b, 1c and 1d) confirm the presence of a spinel structure that match with the JCPDS file of Franklinite (JCPDS 22-1012) together with some amount of ZnO (JCPDS 36-1451), α-Fe2O3 (JCPDS 33-0664) and an amorphous phase. Table 1 gives the structural parameter of sample SG.

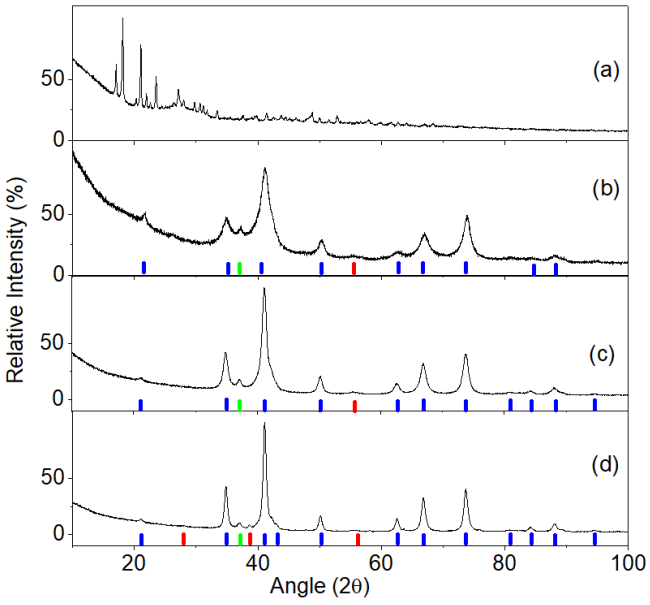

Figure 1: X-ray diffraction patterns of the sol-gel sample (a) as synthetized and after 2 h calcination at (b) 300, (c) 425 (d) 550 ºC. Red, green and blue bars peaks, correspond to α-Fe_2O_3, ZnO and $ZnFe_2O_4$, respectively.

Fig. 2 shows the FTIR spectrum of the precursor and calcined samples in the wave-number range between 500 and 4000 cm^{-1}. As observed in Fig. 2(a), the precursor presents several bands:

a) The large and broad peak at 3465 cm^{-1} resulting from the stretching and deformation vibrations of the water molecules coordinated to the ferrite structure.[51]

b) The characteristic vibrations at 2950 and 2850 cm^{-1} are attributed to the stretching of asymmetric and symmetric vibrations of (–CH_2–) group.[51]

c) The bands at 1685 and 1390 cm^{-1} correspond to the carboxylic anions (COO^-) coordinated by the metal cations, and as the difference between their frequencies is about 295 cm^{-1}, it is suggested a bidentate coordination between the carboxylate and metal ion.[52] Looking in more detail the band at around 1400 cm^{-1}, it is observed that it is actually composed by three overlapping peak, and the other two contributions could be attributed to the stretching vibration of the antisymmetric NO_3 and O-H groups.[53]

d) In the domain 1200 to 600 cm^{-1} the precursor spectrum present bands corresponding to symmetric stretching mode of C-O-C group (1075 cm^{-1}), and to the C-C (900 cm^{-1}) and the wagging mode of C-O bond (780 cm^{-1}).[54]

e) The high intensity band observed in the 670-400 cm^{-1} domain was assigned to the stretching modes of metal-oxygen bonds.

The vibrational spectra of the absorption bands of the samples calcined at 300, 425 and 550 ºC showed the progressive disappearance of the peaks in the range from 900 to 1800 cm^{-1} and 2400 to 3700 cm^{-1}, as observed in the FTIR spectra of Fig 2b, 2c and 2d, confirming the elimination of the stretching mode of organic part during calcination. Besides the presence of some remaining organic sources, these figures show the existence of two mean absorption bands at 425 cm^{-1} and at 575 cm^{-1}, which are attributed to the stretching vibration of the octahedral and tetrahedral metal-oxygen bond, respectively.[55]

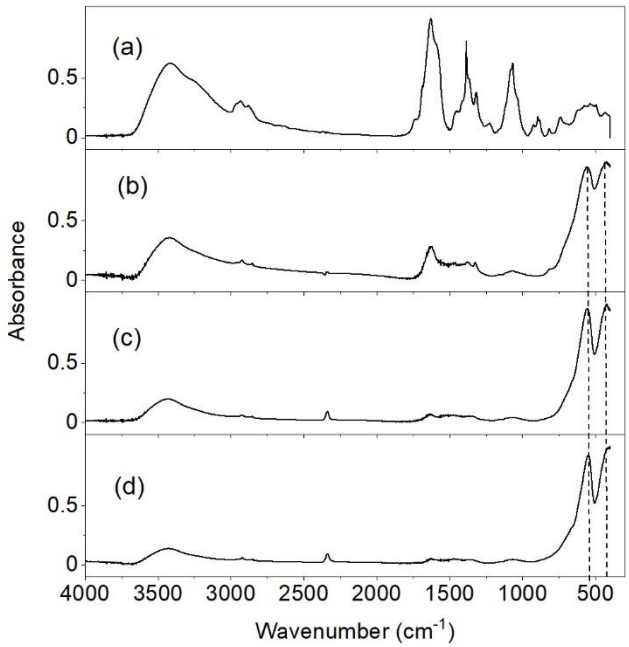

Figure 1: FTIR spectra of the sol-gel sample in (a) as synthetized condition and after 2 h calcination at (b) 300, (c) 425 and (d) 550 ºC. The dotted lines indicate the stretching vibration of the octahedral and tetrahedral metal-oxygen bonds.

In order to understand the reduction process of the sol-gel precursor, it was carried out simultaneous TGA and DSC measurements in the range from 50 to 1200 ºC at 10 K/min. During heating, the TGA curve of Fig. 3 presents a four steps weight loss, with an initial loss of ~20% associated with a broad slightly endothermic peak in DSC in the temperature range from RT to 200 ºC, which was attributed to absorbed water release. A second weight loss of ~37% with a strong and broad exothermic peak was observed in the temperature range from 200 to 320 ºC due to the decomposition of hydroxides and nitrates. On further heating, it was observed a weight loss of ~5% with an small exothermic peak in the temperature range from 320 to 370 ºC. The comparison of the FTIR spectra of samples calcined at 300 and 425ºC (Fig. 2b and 2c) suggests the elimination of almost all the residual organic sources in this temperature range. Finally, it was found a weight loss of ~3% with a very small exothermic peak between 450 and 525 ºC that can be related to further crystallization from an amorphous phase since the FTIR of the sample calcined at 425 and 550ºC are almost identical. As far as no further distinguishable weight loss and peaks on the DSC curve were observed between 525 and 1200 ºC, it was concluded that the combustion and transformation process have been already completed.

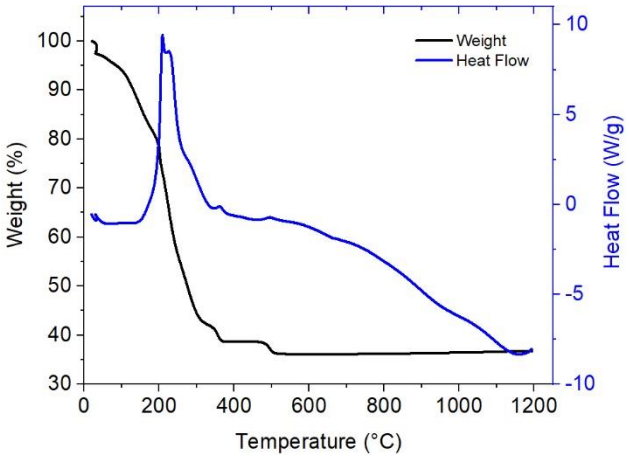

Figure 2: TGA and DSC measurements of the sol-gel precursor

This FTIR analysis together with TGA and DSC curves were very useful for establishing the calcination temperature of 600 ºC to remove unwanted organic ions that may pollute the crystal lattice during preparation and to obtain a high crystalline sample.

The XRD, FTIR, TGA and DSC measurements were also performed in the provided zinc ferrite sample, as shown in Fig. 4a, 4b and 4c. Although the XRD pattern of Figure 4a shows only the presence of zinc ferrite, IR analysis and TG curves confirm the presence of some organic sources.

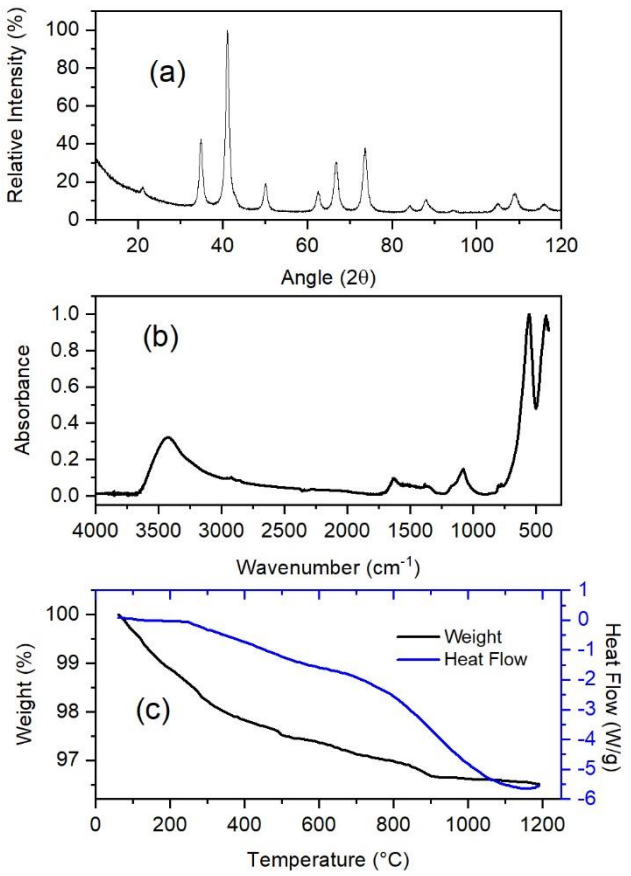

Figure 3: (a) XRD pattern, (b) FTIR spectrum and (c) TGA and DSC measurements obtained for ZFS.

The morphological characteristics of the zinc ferrite powder obtained by the different processing routes were investigated by SEM and TEM. The particle size varies substantially for the different samples due to a different kinetics of the crystal growth for each processing route. As shown in SEM images of Fig. 5a, it was observed the presence of very coarse particles produced in the ceramic route due to the high temperature of the synthesis and the low volume fraction of second phase particles that can pin the grain boundaries. On the other hand, nanometric particles were obtained by the other processing routes including the material supplied by Alfa Aesar. These particles are aggregated, and so it is difficult to determine their exact size and shape. Hence, the exact size and shape of the $ZnFe_2O_4$ particles were examined by TEM images. Figure 5b and 5c shows the typical bright field TEM image of zinc ferrite nanoparticles obtained by sol-gel and mechanochemical synthesis. It can be seen in these TEM image that the zinc ferrite nanoparticles are essentially spherical.

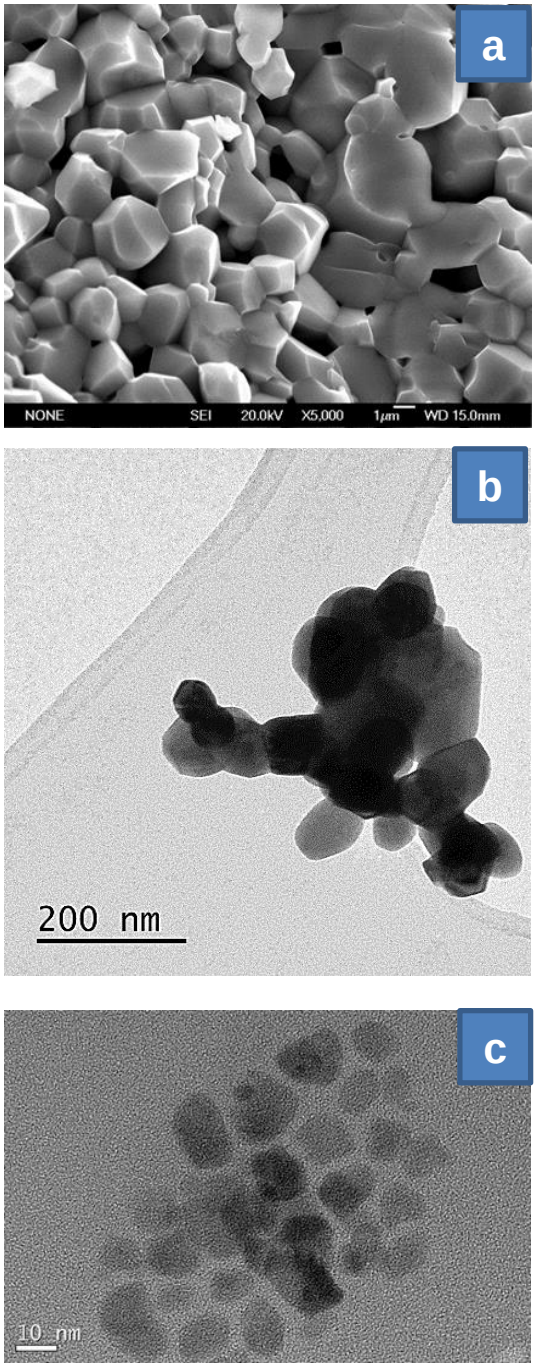

Figure 4: Micrographs of zinc ferrites: (a) SEM images of particles prepared by the conventional ceramic route, (b) TEM images of particles prepared by the sol-gel and (c) mechanochemical synthesis methods

Independently of the preparation method used for their synthesis, the diffraction peaks in the XRD patterns show the presence of a spinel structure, and the EDX measurement confirmed that the Zn to Fe ratio was about 1 to 2, as can be seen in Fig. 1S and Table 1S of the supporting information. However, the samples prepared by the sol-gel and ceramic methods are not monophasic, and they can

include some reflections corresponding to ZnO and α-Fe_2O_3. On the other hand, XRD patters of the samples by mechanochemical synthesis and the rest of the samples mechanically milled for 50 h included beside the zinc ferrite about 1.3% of Fe contamination with the grinding material. Only the sample supplied by Alfa Aesar can be considered as pure zinc ferrite since their XRD patterns showed only the presence of $ZnFe_2O_4$.

The most important microstructural parameter of zinc ferrite determined from the XRD patterns using Rietveld refinement are summarized in Table 1. This table shows that the crystallite size, microstrain and lattice parameter for zinc ferrite prepared by mechanochemical synthesis and for the samples mechanically milled for 50 h are essentially the same. On the other hand, the inversion degree for these samples, defined as the fraction of A-sites occupied by Fe^{3+}, reaches a value close to 0.6 in all samples (see Table 1), suggesting a random distribution of both Fe^{3+} cations between A and B sites.

Table 1. Microstructural parameters obtained after Rietveld refinement of the XRD patterns. The numbers in parenthesis represent the standard deviations. The sample names are CS (ceramic synthesis), SG (sol-gel), ZFS (supplied by Alfa Aesar) and MS (mechanochemical synthesis).

Samples	Lattice parameter (Å)	Inversion parameter	Crystallite size, (nm)	Microstrain	O Position (x=y=z)	Other phases present (%)
As prepared samples						
CS	8.4424(5)	0.14(1)	>150	-	0.242(2)	1.1 ZnO
SG - 600 ºC	8.4439(5)	0.10(1)	24(2)	0.0005(1)	0.241(2)	4.1 ZnO 4.8 Fe_2O_3
ZFS	8.4469(5)	0.25(1)	8.2(5)	0.0010(2)	0.242(2)	--
Milled samples						
MS – 150 h	8.4326(5)	0.56(1)	12(1)	0.0010(2)	0.247(2)	1.3 Fe
CS - 50 h	8.4308(5)	0.61(1)	12(1)	0.0013(2)	0.247(2)	1.3 Fe
SG - 38 h	8.4372(5)	0.56(1)	12(1)	0.0011(2)	0.246(2)	1.6 Fe 2.1 Fe_2O_3
ZFS – 50 h	8.4314(5)	0.56(1)	15 (1)	0.0019(2)	0.246(2)	1.2 Fe

3.2 Magnetic characterization

To understand the nature of magnetic behavior, the temperature dependence of the magnetization under ZFC-FC procedure was measured. As shown in Fig. 6, there is a clear difference between the thermal dependence of ZFC-FC curves

for the different samples which are given by the differences in inversion degree and crystallite sizes. The samples synthesized by ceramic method have the largest crystallite size (>150 nm) and a relative low inversion degree (δ =0.14), this sample shows a cusp a T = 20 K and a splitting of the ZFC from the FC at irreversible temperature T_{irr} ~ 200 K. Even though this curve resembles a antiferromagnetic behavior of the zinc ferrite, the temperature of the cusp is much higher than the Néel temperature of $ZnFe_2O_4$, T_N ~ 11 K.[56] It is worth noting that this sample shows a 14% inversion degree, the exchange of Fe^{3+} from the B to A sites gives place to a spin frustration that leads to spin glass behavior and shifts the maximum of the thermal curves to higher temperatures. In fact, T_{irr} is also related to the observation of spin glass behavior in a system with different sizes of magnetic frustrated clusters.[57] On the other side, the sample provided by Alfa Aesar presents a higher inversion degree (δ~0.25) and much smaller crystallite size (d = 8 nm). As can be seen in Fig. 6b, the maximum of the ZFC curves is displaced to higher temperature (T ~40 K) and T_{irr} is also close to this value. This is consistent with a nanostructured system with a non-negligible value of inversion degree.[31] Regarding the sol-gel sample, the inversion degree is δ~0.10 and particle size d = 24 nm, i.e, smaller inversion degree and higher particle size should shift the maximum of the ZFC-FC to smaller temperatures; however, it has the opposite behavior. This is probable a consequence of the presence of 5% of α-Fe_2O_3 of about 80 nm which can mask the behavior of the zinc ferrite.

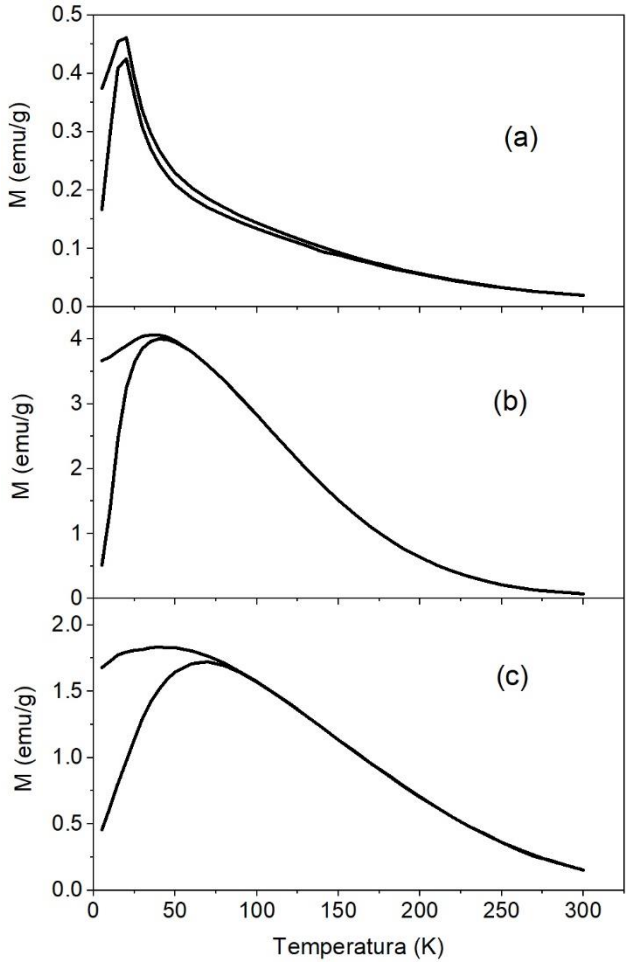

Figure 5: ZFC-FC curves at 100 Oe for (a) CS, (b) ZFS and (c) SG.

ZFC-FC curves of the milled samples are shown in Fig. 7. As it can be seen, after milling, all the samples show similar behavior, with blocking temperature above room temperature. This is related to the fact that, after milling, all the samples have quite similar inversion degree and particle sizes.

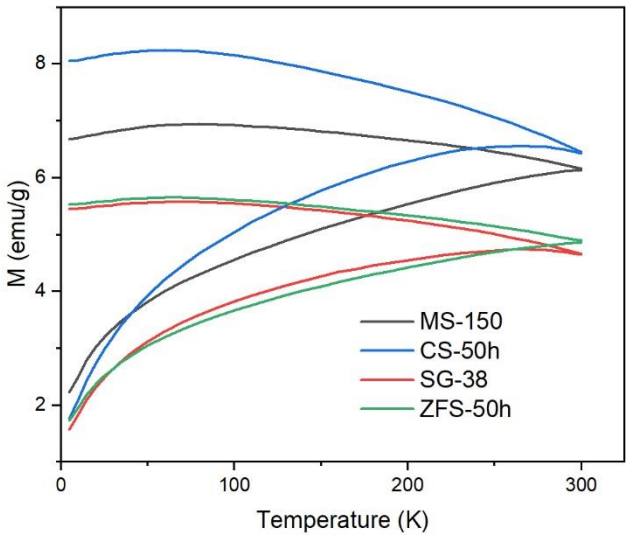

Figure 6: ZFC-FC curves at 100 Oe for mechanochemical synthesis during 150 h milling, sol-gel milled during 38 h, ceramic synthesis and sample supplied by Alfa Aesar milled during 50 h. CS: Ceramic sample, SG: Sol-Gel, ZFS: Zinc Ferrite sample, MS: Mecano-chemical sample.

Magnetic hysteresis measurements of the samples are shown in Fig. 8 and 9 and included in Table 2. At room temperature, only the samples prepared by the conventional ceramic exhibits a paramagnetic behavior characterized by a very feeble magnetization and a magnetic susceptibility χ=1.48(1) emu/g·Oe (Fig. 9a). The sample supplied by Alfa Aesar show an "S" shape with no coercivity and maximum magnetization 17 emu/g achieved at 50 kOe which is consistent with a nanostructured material with non-negligible inversion degree (see Table 1). Sample synthesized by sol-gel shows two contributions: one paramagnetic contribution with χ=1.23(1) emu/g·Oe, and the second one corresponds to a superparamagnetic contribution with M_s = 2 emu/g, which can be associated to the 5% of α-Fe_2O_3 in this sample. On the other hand, Fig. 9b shows that the magnetization curves at room temperature for the samples milled for 50 h are very similar to that of the sample prepared by mechanochemical synthesis, which was expected for the similar values for the microstructural parameters observed in Table 1.

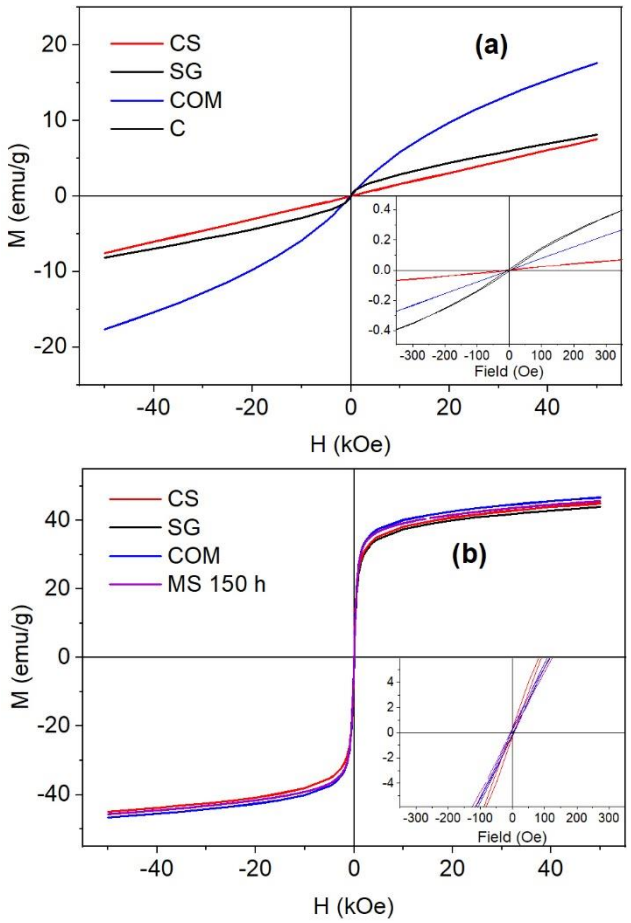

Figure 7: Hysteresis loops measured at 300 K for (a) the samples prepared by different methods and (b) the same samples milled for 50 h. The sample prepared by mechanosynthesis is also shown with a purple line. The insets show the hysteresis curves at low fields. CS: Ceramic sample, SG: Sol-Gel, ZFS: Zinc Ferrite sample, MS: Mecano-chemical sample

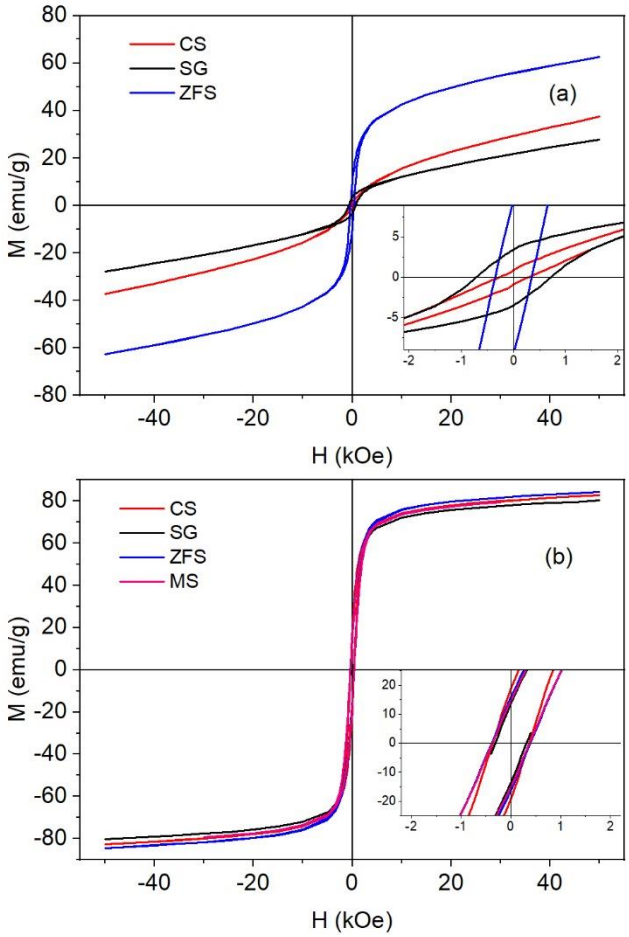

Figure 8: Hysteresis loops measured at 5 K for (a) the samples prepared by different methods and (b) the same samples milled for 50 h. The sample prepared by mechanochemical is also shown with a purple line. The insets show the hysteresis curves at low fields. CS: Ceramic sample, SG: Sol-Gel, ZFS: Zinc Ferrite sample, MS: Mecano-chemical sample

Table 2: Magnetic and structural parameters for all the samples. The saturation magnetization Ms, coercive field Hc, inversion degree, crystallite size d and content of other magnetic phases (Fe and/or hematite). The standard deviations are in parenthesis. CS: Ceramic sample, SG: Sol-Gel, ZFS: Zinc Ferrite sample, MS: Mecano-chemical sample

Sample	**M_s (emu/g)**		**H_c (Oe)**		**δ**	**Cryst. size (nm)**	**α-Fe / α-Fe_2O_3 (%)**
	5 K	**300 K**	**5 K**	**300 K**			
As prepared Samples							
CS	37.4(1)	7.5(1)	290(1)	0	0.14(1)	>150	-
SG-600 ºC	27.8(1)	8.2(1)	700(1)	0	0.10(1)	24(2)	4.8
ZFS	62.5(1)	17.6(1)	350(1)	0	0.25(1)	8.2(5)	-
Milled samples							
CS-50h	79.0(1)	45.3(1)	366(1)	0	0.61(1)	12(1)	1.3
SG-50h	80.1(1)	44.1(1)	295(1)	0	0.56(1)	12(1)	1.6/2.1
ZFS-50h	84.3(1)	46.6(1)	390(1)	0	0.56(1)	15 (1)	1.2
MS-150	79.2(1)	45.6(1)	370(1)	0	0.56(1)	12(1)	1.3

As non-magnetic Zn^{2+} ions are not expected to contribute to the magnetic behavior of the samples, the magnetization is ascribed to Fe^{3+} ions, which present a large magnetic moment of 5.9 μ_B associated to their individual high-spin $Fe^{3+}(d^5)$ ion configuration. It has been observed from neutron diffraction studies that zinc ferrite with an inversion value near to 0.1-0.2, the antiferromagnetic order changes to a ferrimagnetic one.[58] Thus, the samples synthetized by the conventional ceramic and sol-gel routes should present a paramagnetic behavior at room temperature, the weak magnetic component in the sample prepared by the sol-gel route is to the impurity of α-Fe_2O_3 phase detected by XRD.

At low temperatures, the magnetic behaviors of the as-prepared samples are quite different. The magnetization at 50 kOe is different for each sample and, besides, any of them reaches the saturation (see Fig. 9a), which implies a different antiferromagnetic contribution for each sample. The high magnetization

of sample supplied sample (Ms = 62.5 emu/g) is a consequence of the small particle size with an inversion degree of 0.25. By subtracting the susceptibility at high field, a ferromagnetic contribution with M_s = 43 emu/g is obtained, i.e, a significant ferromagnetic component is present[31] that improves the maximum magnetization.

The coercivity of samples CS and ZFS are 290 and 350 Oe, respectively, whereas it increases up to 690 Oe in SG. The high coercivity of sample SG could be given by an exchange interaction between the α-Fe_2O_3 and antiferromagnetic $ZnFe_2O_4$ that enhances the coercive field.

On the other hand, it can be seen that the samples milled during 50 h presents all similar saturation magnetization and coercive fields (see Table 2 and Fig. 9b). The presence of Fe^{+3} ions in both tetrahedral and octahedral sites in the rest of the samples will produce uncompensated moments, giving rise to a ferrimagnetic behavior that enhances the saturation magnetization. Thus, cation inversion is the most important parameters that can be effective in the variation of the magnetic properties of zinc ferrite from the properties of the bulk form. Comparing the results of Tables 1 and 2, and Fig. 9b, the presence of an amount of Fe^{3+} ions in tetrahedral higher than 0.2 gives rise to a ferrimagnetic behavior that enhances the saturation magnetization, associate to inter-sub-lattice AB super-exchange interaction stronger than AA and BB interactions and depends on distances and angles between magnetic cations.[59]

Figure 10 shows that Ms calculated from the hysteresis curves at 5 K after substraction of AFM or PM contributions increases with inversion degree. As Fe^{+3} has a magnetic moment of 5.9μ_B and Zn^{2+} has a zero magnetic moment, Ms should follow the relationship Ms=δ 5.9μ_B which counts for the ratio of Fe^{3+} in A sites. As can be seen in Fig. 10, Ms varies lineally with δ following with a slope close to this value.

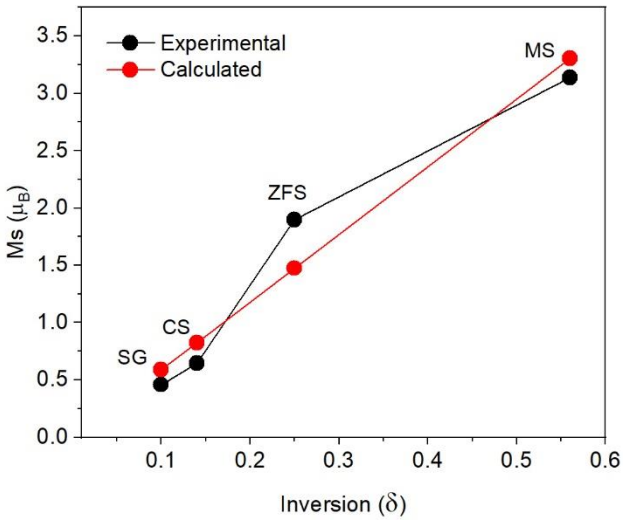

Figure 10: Experimental values of Ms per Bohr magneton as a function inversion degree (δ) (black circles) and calculated as Ms = δ 5.9μ_B (red circles). SG: Sol-Gel, CS: Ceramic, ZFS: zin ferrite supplied, MS: Mechanochemical synthesis.

4. Conclusions

In this work, the magnetic and structural properties of Zn ferrites prepared by ceramic synthesis, sol-gel and mechanochemical synthesis as well as a one provided by a supplier have been investigated. Structural and magnetic studies performed on spinel zinc ferrites prepared by different method of synthesis showed that deviation of their magnetic properties is associated mainly with the cation inversion degree δ. As δ is lower than 0.2 for the samples synthetized by the conventional ceramic or sol-gel routes, they should present a paramagnetic behaviour at room temperature, but due to the presence of some amount of α-Fe_2O_3 phase, the sample prepared by the sol-gel route has a weak magnetic component. On the other hand, the higher inversion degree and much smaller crystallite size showed by the sample provided by Alfa Aesar present a significant ferromagnetic component at low temperatures.

The ZFC-FC curves of the as-prepared samples show that microstructural parameters, such as the inversion degree and the crystallite size as well as the presence of impurities, play a fundamental role in thermal behaviour. On the other hand, ZFC-FC curves of the samples milled for 50 h show similar behaviour to that of the sample prepared by mechanochemical synthesis, with blocking temperature above room temperature, since their microstructure consist of a

single phase spinel ferrite with an almost random distribution of Fe^{3+} and Zn^{2+} cations in both tetrahedral and octahedral sites, that makes the ferrimagnetic interactions are dominant.

Ms calculated from the hysteresis curves at 5 K after subtraction of AFM or PM contributions follow for all samples the relationship $Ms=\delta\ 5.9\mu_B$ which counts for the ratio of Fe^{3+} in A sites.

Finally, it has been observed that, after long milling time, all the samples show the same microstructural and magnetic properties, independently of the initial synthesis route.

CRediT: **MA Cobos:** investigation, visualization, data curation. **P de la Presa:** conceptualization, methodology, resources, writing - review & editing, Funding acquisition, **I Llorente:** formal analysis, software, **A García-Escorial:** validation, review & editing, **A Hernando:** supervision, **JA Jimenez:** conceptualization, methodology, resources, software, writing – original draft, funding acquisition.

Acknowledgements: The authors acknowledge the technical support given by Fernando Giacomone financed by Spanish Ministery of Science and Innovation, PTA2015-10497-I.

Funding: This research was funded by Ministerio de Economía y Competitividad (MINECO) grant number RTI2018-095856-B-C21 and by by Madrid Region grant number S2018/NMT-4381-MAT4.0-CM.

References

[1] H.S.C. Oneill, A. Navrotsky, Simple spinels - crystallographic parameters, cation radii, lattice energies and cation distribution, American Mineralogist, 68 (1983) 181-194.
[2] B. Lavina, G. Salviulo, A.D. Giusta, Cation distribution and structure modelling of spinel solid solutions, Physics and Chemistry of Minerals, 29 (2002) 10-18.
[3] J.M. Hastings, L.M. Corliss, An Antiferromagnetic Transition in Zinc Ferrite, Physical Review, 102 (1956) 1460-1463.
[4] W. Schiessl, W. Potzel, H. Karzel, M. Steiner, G.M. Kalvius, A. Martin, M.K. Krause, I. Halevy, J. Gal, W. Schäfer, G. Will, M. Hillberg, R. Wäppling, Magnetic properties of the Zn${\mathrm{Fe}}_{2}$${\mathrm{O}}_{4}$ spinel, Physical Review B, 53 (1996) 9143-9152.
[5] Y. Yamada, K. Kamazawa, Y. Tsunoda, Interspin interactions in ${\mathrm{ZnFe}}_{2}{\mathrm{O}}_{4}:$ Theoretical analysis of neutron scattering study, Physical Review B, 66 (2002) 064401.

[6] V. Šepelák, L. Wilde, U. Steinike, K.D. Becker, Thermal stability of the non-equilibrium cation distribution in nanocrystalline high-energy milled spinel ferrite, Materials Science and Engineering: A, 375-377 (2004) 865-868.
[7] S.J. Stewart, S.J.A. Figueroa, M.B. Sturla, R.B. Scorzelli, F. Garcia, F.G. Requejo, Magnetic ZnFe2O4 nanoferrites studied by X-ray magnetic circular dichroism and Mossbauer spectroscopy, Physica B, 389 (2007) 155-158.
[8] S.H. Yu, T. Fujino, M. Yoshimura, Hydrothermal synthesis of ZnFe2O4 ultrafine particles with high magnetization, J. Magn. Magn. Mater., 256 (2003) 420-424.
[9] H.S. Oneill, TEMPERATURE-DEPENDENCE OF THE CATION DISTRIBUTION IN ZINC FERRITE (ZNFE2O4) FROM POWDER XRD STRUCTURAL REFINEMENTS, Eur. J. Mineral., 4 (1992) 571-580.
[10] C.B.R. Jesus, E.C. Mendonca, L.S. Silva, W.S.D. Folly, C.T. Meneses, J.G.S. Duque, Weak ferromagnetic component on the bulk ZnFe2O4 compound, J. Magn. Magn. Mater., 350 (2014) 47-49.
[11] M. Veverka, Z. Jirak, O. Kaman, K. Knizek, M. Marysko, E. Pollert, K. Zaveta, A. Lancok, M. Dlouha, S. Vratislav, Distribution of cations in nanosize and bulk Co-Zn ferrites, Nanotechnology, 22 (2011) 7.
[12] R. Vinas, I. Alvarez-Serrano, M.L. Lopez, C. Pico, M.L. Veiga, F. Mompean, M. Garcia-Hernandez, Influence of particle sizes on the electronic behavior of ZnxCo1- xFe(2)O(4) spinels (x=0.2, 0.3), Journal of Alloys and Compounds, 601 (2014) 130-139.
[13] B.P. Rao, C.O. Kim, C. Kim, I. Dumitru, L. Spinu, O.F. Caltun, Structural and magnetic characterizations of coprecipitated Ni-Zn and Mn-Zn ferrite nanoparticles, Ieee Transactions on Magnetics, 42 (2006) 2858-2860.
[14] M. Maletin, E.G. Moshopoulou, V.V. Srdic, Magnetic properties of ZnFe2O4 and In-doped ZnFe2O4 nanoparticles, Physica Status Solidi a-Applications and Materials Science, 205 (2008) 1831-1834.
[15] P.M.P. Swamy, S. Basavaraja, A. Lagashetty, N.V.S. Rao, R. Nijagunappa, A. Venkataraman, Synthesis and characterization of zinc ferrite nanoparticles obtained by self-propagating low-temperature combustion method, Bulletin of Materials Science, 34 (2011) 1325-1330.
[16] L.R. Gonsalves, S.C. Mojumdar, V.M.S. Verenkar, Synthesis and characterization of ultrafine spinel ferrite obtained by precursor combustion technique, Journal of Thermal Analysis and Calorimetry, 108 (2012) 859-863.
[17] R. Verma, S.N. Kane, P. Tiwari, S.S. Modak, T. Tatarchuk, F. Mazaleyrat, Ni addition induced modification of structural, magnetic properties and antistructural modeling of Zn1-xNixFe2O4 (x = 0.0 - 1.0) nanoferrites, Molecular Crystals and Liquid Crystals, 674 (2018) 130-141.
[18] M.H. Habibi, A.H. Habibi, Effect of the thermal treatment conditions on the formation of zinc ferrite nanocomposite, ZnFe2O4, by sol-gel method, Journal of Thermal Analysis and Calorimetry, 113 (2013) 843-847.
[19] R.P. Patil, S.D. Delekar, D.R. Mane, P.P. Hankare, Synthesis, structural and magnetic properties of different metal ion substituted nanocrystalline zinc ferrite, Results in Physics, 3 (2013) 129-133.
[20] T. Tatarchuk, M. Myslin, I. Mironyuk, M. Bououdina, A.T. Pędziwiatr, R. Gargula, B.F. Bogacz, P. Kurzydło, Synthesis, morphology, crystallite size and adsorption properties of nanostructured Mg–Zn ferrites with enhanced porous structure, Journal of Alloys and Compounds, 819 (2020) 152945.
[21] K. Praveena, K. Sadhana, S. Bharadwaj, S.R. Murthy, Development of nanocrystalline Mn-Zn ferrites for high frequency transformer applications, J. Magn. Magn. Mater., 321 (2009) 2433-2437.
[22] S.J. Stewart, I.A. Al-Omari, F.R. Sives, H.M. Widatallah, Non-equilibrium cation influence on the Neel temperature in ZnFe2O4, Journal of Alloys and Compounds, 495 (2010) 506-508.

[23] R. Shu, J. Zhang, Y. Wu, Z. Wan, M. Zheng, Facile design of nitrogen-doped reduced graphene oxide/zinc ferrite hybrid nanocomposites with excellent microwave absorption in the X-band, Materials Letters, 255 (2019) 126549.
[24] R. Shu, G. Zhang, X. Wang, X. Gao, M. Wang, Y. Gan, J. Shi, J. He, Fabrication of 3D net-like MWCNTs/ZnFe2O4 hybrid composites as high-performance electromagnetic wave absorbers, Chemical Engineering Journal, 337 (2018) 242-255.
[25] R. Shu, J. Zhang, C. Guo, Y. Wu, Z. Wan, J. Shi, Y. Liu, M. Zheng, Facile synthesis of nitrogen-doped reduced graphene oxide/nickel-zinc ferrite composites as high-performance microwave absorbers in the X-band, Chemical Engineering Journal, 384 (2020) 123266.
[26] J.W. Mao, X.H. Hou, H.D. Chen, Q. Ru, S.J. Hu, K.H. Lam, Facile spray drying synthesis of porous structured ZnFe2O4 as high-performance anode material for lithium-ion batteries, Journal of Materials Science-Materials in Electronics, 28 (2017) 3709-3715.
[27] R. Dom, R. Subasri, N.Y. Hebalkar, A.S. Chary, P.H. Borse, Synthesis of a hydrogen producing nanocrystalline ZnFe2O4 visible light photocatalyst using a rapid microwave irradiation method, Rsc Advances, 2 (2012) 12782-12791.
[28] M. Niyaifar, Effect of Preparation on Structure and Magnetic Properties of ZnFe2O4, Journal of Magnetics, 19 (2014) 101-105.
[29] V. Nachbaur, G. Tauvel, T. Verdier, M. Jean, J. Juraszek, D. Houvet, Mecanosynthesis of partially inverted zinc ferrite, Journal of Alloys and Compounds, 473 (2009) 303-307.
[30] S.J. Stewart, S.J.A. Figueroa, J.M. Lopez, S.G. Marchetti, J.F. Bengoa, R.J. Prado, F.G. Requejo, Cationic exchange in nanosized ZnFe2O4 spinel revealed by experimental and simulated near-edge absorption structure, Physical Review B, 75 (2007) 4.
[31] M.A. Cobos, P. de la Presa, I. Llorente, J.M. Alonso, A. Garcia-Escorial, P. Marin, A. Hernando, J.A. Jimenez, Magnetic Phase Diagram of Nanostructured Zinc Ferrite as a Function of Inversion Degree delta, Journal of Physical Chemistry C, 123 (2019) 17472-17482.
[32] H.H. Hamdeh, J.C. Ho, S.A. Oliver, R.J. Willey, G. Oliveri, G. Busca, Magnetic properties of partially-inverted zinc ferrite aerogel powders, Journal of Applied Physics, 81 (1997) 1851-1857.
[33] F.S. Li, L. Wang, J.B. Wang, Q.G. Zhou, X.Z. Zhou, H.P. Kunkel, G. Williams, Site preference of Fe in nanoparticles of ZnFe2O4, J. Magn. Magn. Mater., 268 (2004) 332-339.
[34] M. Mozaffari, M.E. Arani, J. Amighian, The effect of cation distribution on magnetization of ZnFe2O4 nanoparticles, J. Magn. Magn. Mater., 322 (2010) 3240-3244.
[35] C.N. Chinnasamy, A. Narayanasamy, N. Ponpandian, K. Chattopadhyay, H. Guerault, J.M. Greneche, Ferrimagnetic ordering in; nanostructured zinc ferrite, Scripta Materialia, 44 (2001) 1407-1410.
[36] C.N. Chinnasamy, A. Narayanasamy, N. Ponpandian, K. Chattopadhyay, K. Shinoda, B. Jeyadevan, K. Tohji, K. Nakatsuka, T. Furubayashi, I. Nakatani, Mixed spinel structure in nanocrystalline NiFe2O4, Physical Review B, 63 (2001) 6.
[37] C.N. Chinnasamy, A. Narayanasamy, N. Ponpandian, K. Chattopadhyay, H. Guerault, J.M. Greneche, Magnetic properties of nanostructured ferrimagnetic zinc ferrite, J. Phys.-Condes. Matter, 12 (2000) 7795-7805.
[38] C. Suryanarayana, Mechanical Alloying: A Novel Technique to Synthesize Advanced Materials, Research, 2019 (2019) 17.
[39] Y.R. Zhu, X.B. Ji, Z.P. Wu, W.X. Song, H.S. Hou, Z.B. Wu, X. He, Q.Y. Chen, C.E. Banks, Spinel NiCo2O4 for use as a high-performance supercapacitor electrode material: Understanding of its electrochemical properties, J. Power Sources, 267 (2014) 888-900.
[40] M. Atif, S.K. Hasanain, M. Nadeem, Magnetization of sol-gel prepared zinc ferrite nanoparticles: Effects of inversion and particle size, Solid State Commun., 138 (2006) 416-421.
[41] F.S. Li, H.B. Wang, L. Wang, J.B. Wang, Magnetic properties of ZnFe2O4 nanoparticles produced by a low-temperature solid-state reaction method, J. Magn. Magn. Mater., 309 (2007) 295-299.

[42] M. Veith, M. Haas, V. Huch, Single source precursor approach for the sol-gel synthesis of nanocrystalline ZnFe2O4 and zinc-iron oxide composites, Chemistry of Materials, 17 (2005) 95-101.
[43] W. Kim, F. Saito, Mechanochemical synthesis of zinc ferrite from zinc oxide and alpha-Fe2O3, Powder Technology, 114 (2001) 12-16.
[44] H.J. Fecht, Nanostructure formation by mechanical attrition, Nanostructured Materials, 6 (1995) 33-42.
[45] K. Kamazawa, Y. Tsunoda, H. Kadowaki, K. Kohn, Magnetic neutron scattering measurements on a single crystal of frustrated ZnFe2O4, Physical Review B, 68 (2003).
[46] Y. Yamada, K. Kamazawa, Y. Tsunoda, Interspin interactions in ZnFe2O4: Theoretical analysis of neutron scattering study, Physical Review B, 66 (2002).
[47] J.M. Quintero, K.L.S. Rodriguez, F.A.G. Albarracin, H.D. Rosales, P.M. Zelis, S.J. Stewart, L.A. Errico, C.R. Torres, On the deviation from a Curie-Weiss behavior of the ZnFe2O4 susceptibility: A combined ab-initio and Monte-Carlo approach, Heliyon, 5 (2019).
[48] P. Villars, K. Cenzual, Pearson's crystal data: crystal structure database for inorganic compounds, in, ASM International®, Materials Park, Ohio, USA, 2019/2020.
[49] D. Balzar, Profile fitting of X-ray diffraction lines and Fourier analysis of broadening, Journal of Applied Crystallography, 25 (1992) 559-570.
[50] D. Balzar, N. Audebrand, M.R. Daymond, A. Fitch, A. Hewat, J.I. Langford, A. Le Bail, D. Louer, O. Masson, C.N. McCowan, N.C. Popa, P.W. Stephens, B.H. Toby, Size-strain line-broadening analysis of the ceria round-robin sample, Journal of Applied Crystallography, 37 (2004) 911-924.
[51] M.I. Loría-Bastarrachea, W. Herrera-Kao, J.V. Cauich-Rodríguez, J.M. Cervantes-Uc, H. Vázquez-Torres, A. Ávila-Ortega, A TG/FTIR study on the thermal degradation of poly(vinyl pyrrolidone), Journal of Thermal Analysis and Calorimetry, 104 (2011) 737-742.
[52] R.A. Bortnic, F. Goga, A. Mesaros, M. Nasui, B.S. Vasile, D. Roxana, A. Avram, SYNTHESIS OF COBALT FERRITE NANOPARTICLES VIA A SOL-GEL COMBUSTION METHOD, Studia Universitatis Babes-Bolyai Chemia, 61 (2016) 213-222.
[53] P. Priyadharsini, A. Pradeep, P.S. Rao, G. Chandrasekaran, Structural, spectroscopic and magnetic study of nanocrystalline Ni–Zn ferrites, Materials Chemistry and Physics, 116 (2009) 207-213.
[54] A.B. Brizuela, L.C. Bichara, E. Romano, A. Yurquina, S. Locatelli, S.A. Brandán, A complete characterization of the vibrational spectra of sucrose, Carbohydrate Research, 361 (2012) 212-218.
[55] G.V.S. Rao, C.N.R. Rao, J.R. Ferraro, INFRARED AND ELECTRONIC SPECTRA OF RARE EARTH PEROVSKITES - ORTHO-CHROMITES, ORTHO-MANGANITES AND ORTHO-FERRITES, Applied Spectroscopy, 24 (1970) 436-&.
[56] J.C. Ho, H.H. Hamdeh, Y.Y. Chen, S.H. Lin, Y.D. Yao, R.J. Willey, S.A. Oliver, Low-temperature calorimetric properties of zinc ferrite nanoparticles, Physical Review B, 52 (1995) 10122-10126.
[57] K.L. Lopez-Maldonado, P. de la Presa, I. Betancourt, J.R. Farias Mancilla, J.A. Matutes Aquino, A. Hernando, J.T. Elizalde Galindo, Superparamagnetic response of zinc ferrite incrusted nanoparticles, Journal of Alloys and Compounds, 637 (2015) 443-448.
[58] M. Hofmann, S.J. Campbell, H. Ehrhardt, R. Feyerherm, The magnetic behaviour of nanostructured zinc ferrite, Journal of Materials Science, 39 (2004) 5057-5065.
[59] A. Goldman, Modern Ferrite Technology, 2nd Edition, Springer +Business media, New York, 2006.